


RESEARCH ARTICLE

Controllable self-transport of bouncing droplets on ultraslippery surfaces with wedge-shaped grooves

Chuchen Yue¹  | Qingwen Dai¹  | Xiaolong Yang¹  | Carsten Gachot²  | Wei Huang¹  | Xiaolei Wang¹ 

¹College of Mechanical and Electrical Engineering, Nanjing University of Aeronautics & Astronautics, Nanjing, China

²Institute of Engineering Design and Product Development, Tribology Research Group, TU Wien, Vienna, Austria

Correspondence

Qingwen Dai, College of Mechanical and Electrical Engineering, Nanjing University of Aeronautics & Astronautics, Nanjing 210016, China.

Email: daiqingwen@nuaa.edu.cn

Funding information

National Natural Science Foundation of China, Grant/Award Number: 51805252; Alexander von Humboldt Foundation

Abstract

Preventing the accretion of droplets on surfaces is vital and slippery liquid-infused porous surfaces (SLIPS) have promising application prospects, such as surface self-cleaning and droplet transportation. In this work, controllable self-transport of bouncing droplets on ultraslippery surfaces with wedge-shaped grooves is reported. The impact behaviors of droplets on SLIPS under various impact velocities and diameters are explored, which can be classified as hover, total bounce, partial bounce, Worthington jet, and crush. SLIPS with wedge-shaped grooves were designed to transport accreted droplets. An energy and transport model is established to explain the impact and self-transport mechanism, where the Laplace pressure and moving resistance between droplets play a key role. Finally, SLIPS with branched wedge-shaped grooves were designed for droplet self-transport and demonstrated advantages. This work provides a general reference for spontaneous motion control of sessile droplets, droplets with initial impacting velocity, or even liquid films.

INTRODUCTION

The separation of droplets after impacting solid surfaces is crucial for certain applications, such as energy harvesting,¹ heat transfer,² surface self-cleaning,³ and so on.⁴ To achieve the solid-liquid separation, different strategies including surface superhydrophobic treatment,⁵ pneumatic programmable surface,⁶ preimpregnated oil films,⁷ and external physical fields⁸ of vibration⁹ have been proposed. Although letting droplets bounce off surfaces is very intuitive, they would still fall back to surfaces. Under those conditions, how to design surfaces to promote the spontaneous movement of accreted droplets is of great significance for droplet-based electricity generators,¹⁰ thermal management,¹¹ and drug transportation.¹² SLIPS offer a possibility to achieve this goal.

The design inspiration for slippery liquid-infused porous surfaces (SLIPS) was from the micro-nano structures and lubricating mucous

membranes in a *Nepenthes* pitcher.¹³ The bionics concept of SLIPS was first introduced in 2011;¹⁴ they have outstanding properties of low surface tension¹⁵ and low sliding angle,¹⁶ on which droplets can slide freely. Moreover, the lubricant inside SLIPS provides excellent self-healing capacity.¹⁷ Thus, SLIPS have attracted considerable attention in applications of anti-icing,¹⁸ self-cleaning,¹⁹ water collection,²⁰ and so on.²¹ Appropriate design of the topography of SLIPS allows one to direct the movement of droplets for achieving solid-liquid separation and improving surface cleaning efficiency,²² of which the wedge-shaped groove is a typical example.^{23–25} Guan et al.²⁶ reported the bidirectional motion of droplets within a wedge-shaped propelled droplet transport and provided a theoretical explanation. Wang et al.²⁷ identified the factors affecting the distance of transport and provided guidelines for wedge-shaped design for optimized spontaneous liquid transport. It is confirmed

Chuchen Yue and Qingwen Dai contributed equally to this work.

This is an open access article under the terms of the [Creative Commons Attribution](https://creativecommons.org/licenses/by/4.0/) License, which permits use, distribution and reproduction in any medium, provided the original work is properly cited.

© 2024 The Authors. *Droplet* published by Jilin University and John Wiley & Sons Australia, Ltd.

that wedge angle and groove depth are two important indicators of wedge-shaped structures.²⁸ Similar to superhydrophobic surfaces, water droplets also show behaviors such as deposition, total bounce, and splashing on impact on SLIPS.^{29,30} A basic question that arises if one wants to use SLIPS for surface cleaning is as follows: is there a possibility to control the self-transport behavior of droplets on SLIPS with wedge-shaped structures?

Hence, in this work, controllable self-transport of bouncing droplets on ultraslippery surfaces with wedge-shaped grooves was investigated. The impact behaviors of droplets on SLIPS were explored. SLIPS with wedge-shaped grooves under different conditions were designed to illustrate the influence of wedge angle and groove depth. Energy and self-transport models were established, and SLIPS with branched wedge-shaped grooves were designed for droplet self-transport and demonstrated advantages. This work provides a general reference for spontaneous motion control of sessile droplets, droplets with initial impacting velocity, or even liquid films.

RESULTS AND DISCUSSION

Figure 1 shows the brief fabrication progress of SLIPS: copper sheets were scanned by a UV-laser marking machine to fabricate nanostructures to improve the adhesion between lubricants and surfaces, and wedge-shaped grooves were produced according to specific requirements. After that, samples were subjected to chemical modification to lower the surface tension and it can be seen from the scanning electron microscope (SEM) that the surface had formed a grid-like microarray, while spherical cluster structures and nano grass-like structures were formed on surfaces, which contribute to the superhydrophobic property, and the contact angle θ_{ca} of the water droplet (5 μ L) was $\sim 166^\circ$. By dripping silicone oil uniformly, SLIPS similar to the *Nepenthes* pitcher can be obtained after draining away excess silicone oil. The contact angle of the water droplet on SLIPS was $\sim 111^\circ$, and the sliding, advancing, and receding angles were 2, 108, and 93° , respectively. SLIPS without grooves and with

grooves were used for droplet impact and transport experiments, respectively.

Figure 2a shows the impact behaviors of water droplets on SLIPS with impact velocity $U = 0.4\text{--}2.5$ m/s and diameter $D = 2.3$ mm. It can be seen that there is hover, Worthington jet, crush, partial bounce, and total bounce. Although there is a phenomenon of solid-liquid separation, droplets eventually deposited on the surface in all cases. To describe the impact conditions, dimensionless capillary ($Ca = \mu U / \gamma$, where γ and μ are the surface tension and viscosity, respectively) and Bond ($Bo = \rho g R_0^2 / \gamma$, where ρ , R_0 , and g are the density, the initial radius of the droplet, and gravitational acceleration, respectively) numbers were introduced. Figure 2b shows the relationship between Bo , Ca , and impact behaviors when droplets impact SLIPS, where the influence parameters of Ca and Bo are U (0.52–0.63 m/s) and R_0 (1.15–1.6 mm), respectively. Droplets undergo a process of hover, total, and partial bouncing with increasing impact velocity, and the corresponding regions are identified by blue, red, and orange colors, respectively. With increasing diameter, different behavior regions could be obtained. Both total bounce ranges (the red area) and the required Ca for it are negatively correlated with Bo .

Inspired by the conical structures of the thorn of cactus, where droplets can transport spontaneously from top to bottom, a wedge-shaped groove with wedge angle θ_a and groove depth h was constructed, as shown in Figure 3a. Figure 3b shows the impact dynamics (side view) of the first step and the subsequent spontaneous transport progress (overhead view) of the droplet with $U = 0$ and $D = 2.7$ mm on SLIPS ($\theta_a = 10^\circ$ and $h = 0.4$ mm; detailed progress can be seen in the Supporting Information: Movies S1 and S2). After spreading and retraction processes, the droplet starts moving in the wedge-shaped groove under the effect of Laplace pressure ΔP , which can be expressed as^{31,32}

$$\Delta P = 2\gamma_{\text{water}} \left(\frac{1}{R_b} - \frac{1}{R_f} \right), \quad (1)$$

where γ_{water} , R_b , and R_f represent the surface tension, and the radius of curvature at the back and front of the droplet, respectively. It was reported that the self-driving force is equated to the Laplace pressure.¹⁵

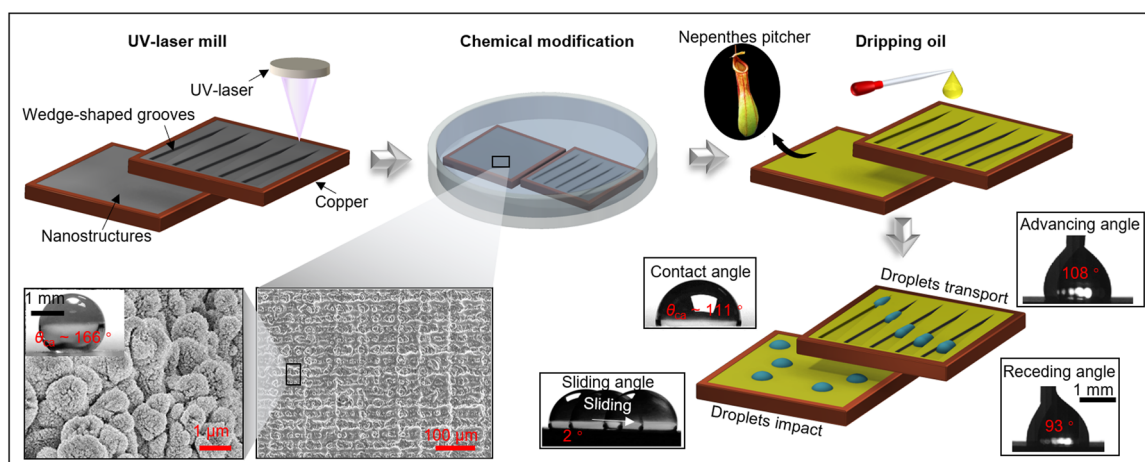


FIGURE 1 Fabrication progress of slippery liquid-infused porous surfaces and the characteristics of water droplets.

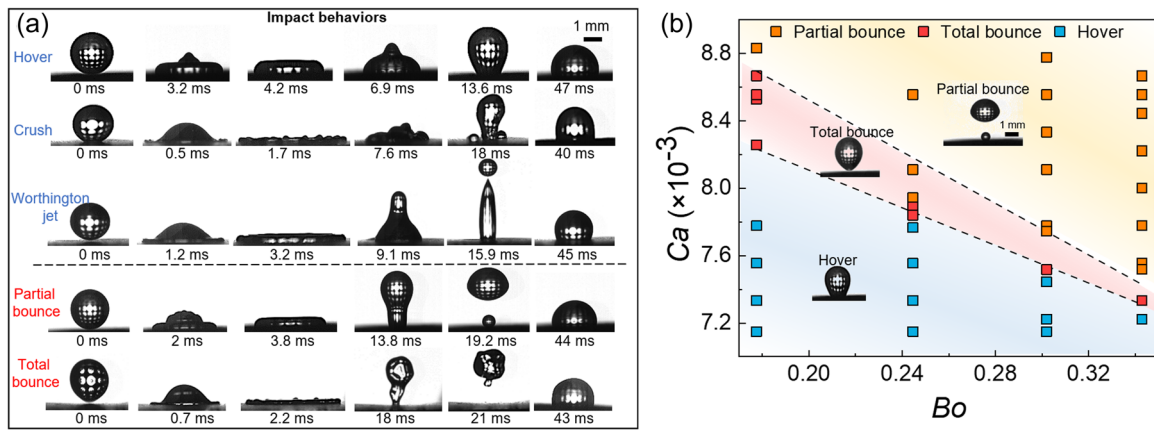


FIGURE 2 Basic impact dynamics. (a) Five impact behaviors of droplets on slippery liquid-infused porous surfaces (SLIPS). (b) Relationship between Ca , Bo , and impact behaviors of droplets on SLIPS.

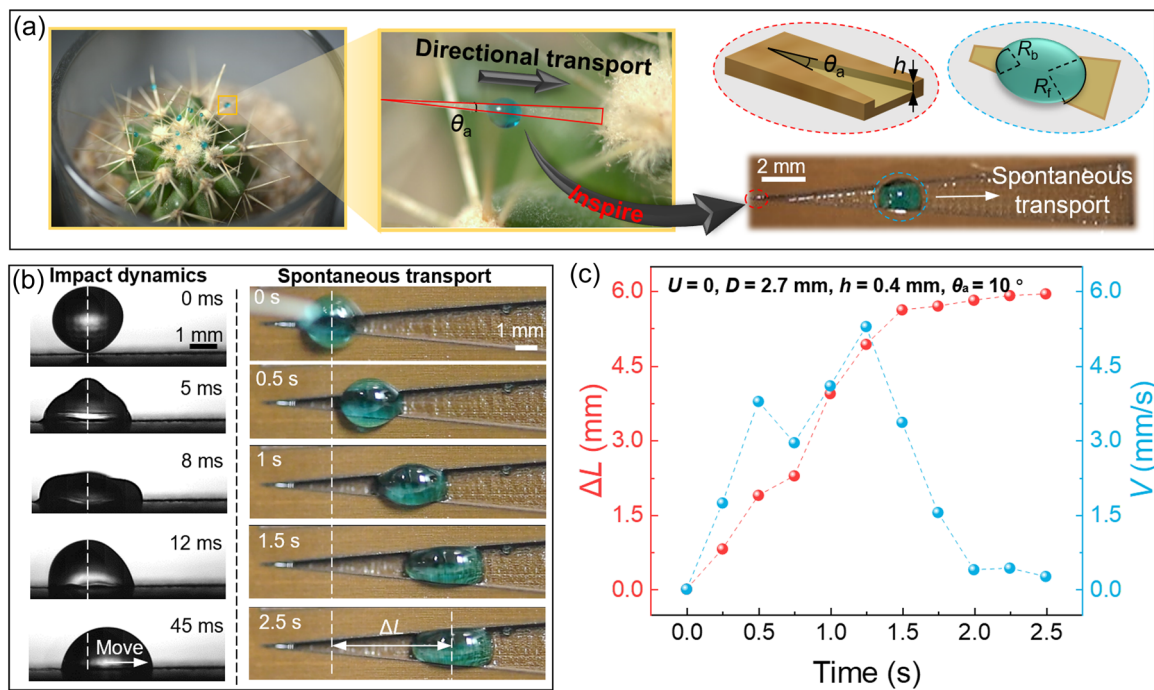


FIGURE 3 Design of wedge-shaped grooves and droplet behaviors. (a) Schematic of the motion configuration of the thorn of cactus and schematic of wedge-shaped grooves on slippery liquid-infused porous surfaces, and parameter definition. (b) Impact dynamics and spontaneous transport. (c) Evolution of ΔL and V as time elapsed.

To describe the transport behavior shown in Figure 3b, the evolution of transport distance ΔL and transport velocity V as time elapsed was measured. It can be seen from Figure 3c that V has two peaks and the distance increases significantly between 0.75 and 1.5 s. As mentioned in the introduction, θ_a and h are the two key parameters for wedge-shaped grooves; thus, parameter optimization was carried out to enhance the droplet spontaneous transport performance.

According to the impacting behaviors shown in Figure 2b, the range of U in experiments was increased from 0 to 0.72 m/s. The influence of D and U on droplet transport with $h = 0.4$ mm and $\theta_a = 10^\circ$ is shown in Figure 4a. It can be observed that the final transport

distance is positively correlated with time, and ΔL decreases first and then increases under different D and U . To assess the effect of wedge angle and groove depth on droplet transport, ΔL and the average transport velocity V_{ave} of the whole transport progress were combined, and an evaluation indicator P was introduced, which can be expressed as

$$P = \frac{\Delta L_{(Ca,Bo)}}{\Delta L_{max(Ca,Bo)}} + \frac{V_{ave(Ca,Bo)}}{V_{avemax(Ca,Bo)}}, \quad (2)$$

where $\Delta L_{(Ca,Bo)}$ and $V_{ave(Ca,Bo)}$ are the transport distance and the average transport velocity when the droplet impacts the groove

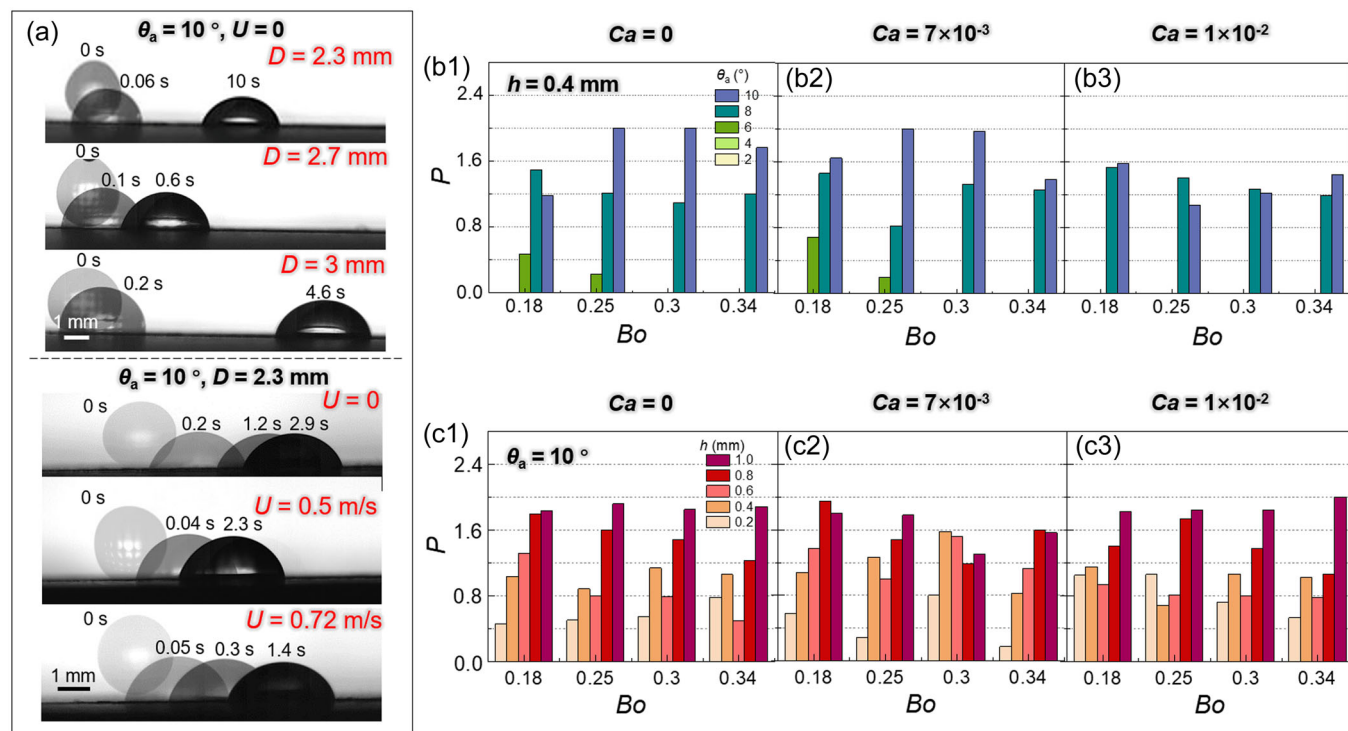


FIGURE 4 Influence of h and θ_a on droplets' spontaneous transport. (a) Transport dynamics of droplets. (b1–b3) Relationship between P and Bo with $h = 0.4 \text{ mm}$ and different Ca and θ_a . (c1–c3) Relationship between P and Bo with $\theta_a = 10^\circ$ and different Ca and h .

($\theta_a = 2, 4, 6, 8$, or 10°), with $Ca = 0, 7 \times 10^{-3}$ or 1×10^{-2} , and $Bo = 0.18, 0.25, 0.3$, or 0.34 , respectively, while $\Delta L_{\max}(Ca, Bo)$ and $V_{\text{avemax}}(Ca, Bo)$ are the max transport distance and the average transport velocity when $\theta_a = 2, 4, 6, 8$, and 10° , with the same Ca and Bo , respectively. It can be observed from Figure 4b1–b3 that $\theta_a = 10^\circ$ shows a better performance on P than $\theta_a = 2, 4, 6$, and 8° . Hence, $\theta_a = 10^\circ$ was selected, and Figure 4c1–c3 shows that the combination of $\theta_a = 10^\circ$ and $h = 1 \text{ mm}$ is the best in most cases.

Once the influence of different θ_a and h on droplet transport efficiency has been determined, the most suitable parameters can be selected based on Ca and Bo . With $Ca = 5.5 \times 10^{-3} - 1.1 \times 10^{-1}$ and $Bo = 0.18 - 0.34$, Figure 5a shows the strategy of efficient droplet separation from SLIPS at different Ca and Bo ; the red area represents complete droplet bouncing, while the blue area represents use of wedge-shaped grooves with different parameter combinations and different legends represent specific parameters. The total bounce area is negatively correlated with Bo , which suggests that larger D is not conducive to complete droplet bouncing. As droplets with larger Bo under the same h and θ_a are subjected to greater viscous resistance to movement, they need larger θ_a for transport. Figure 5b shows the morphology and energy change process of the droplet when $Ca = 7 \times 10^{-3}$ and $Bo = 0.18$. Because of the existence of adhesion between the liquid film and the droplet,³³ the initial kinetic energy E_k and gravitational potential energy E_g would be used to overcome the resistance and thus dissipate in the form of viscous dissipation W_v and interfacial friction W_f , but most of them are converted into the surface energy E_s while turning back when the

droplet starts to retract.³⁴ Figure 5c1 shows the spontaneous transport of the droplet in the wedge-shaped groove, where it shows progress from unfolding to stationary when $Ca = 1 \times 10^{-2}$ and $Bo = 0.18$. It can be seen from Figure 5c2 that at the beginning of transport, the symmetrical shape can be maintained and the difference between the left and right liquid–gas surface tension, that is, γ_{LG} and γ'_{LG} , is small due to the small volume of the droplet in the groove, where the driving force F_L , which is approximately equal to ΔP , overcomes the moving resistance F_{re} , which is known as the Fumridge equation³⁵

$$F_{re} = \gamma_{wo} W_{dp} (\cos \theta_R - \cos \theta_A), \quad (3)$$

where γ_{wo} is the surface tension of the interface between water and silicone oil, W_{dp} is the interfacial width of the droplet perpendicular to the moving direction, and θ_R and θ_A represent receding and advancing contact angles, respectively.³⁶ Due to the different widths of the front and back grooves, the front of the droplet is subjected to a greater driving force that undergoes asymmetric deformation as shown in Figure 5c1 (the continuous process can be seen in the Supporting Information: Movie S3). As the driving force and the viscous drag between water and oil balance each other, the droplet stops moving and once again regains its symmetrical shape. As time elapses, the sinking leads to lateral elongation of the droplet, where the capillary flow generated by the increase of the difference between γ_{LG} and γ'_{LG} weakens F_L .²⁴ At last, F_{re} is equal to F_L and the droplet stops moving since W_{dp} continuously increases as the droplet moves forward, at the same time γ_{LG} and γ'_{LG} become equal again.

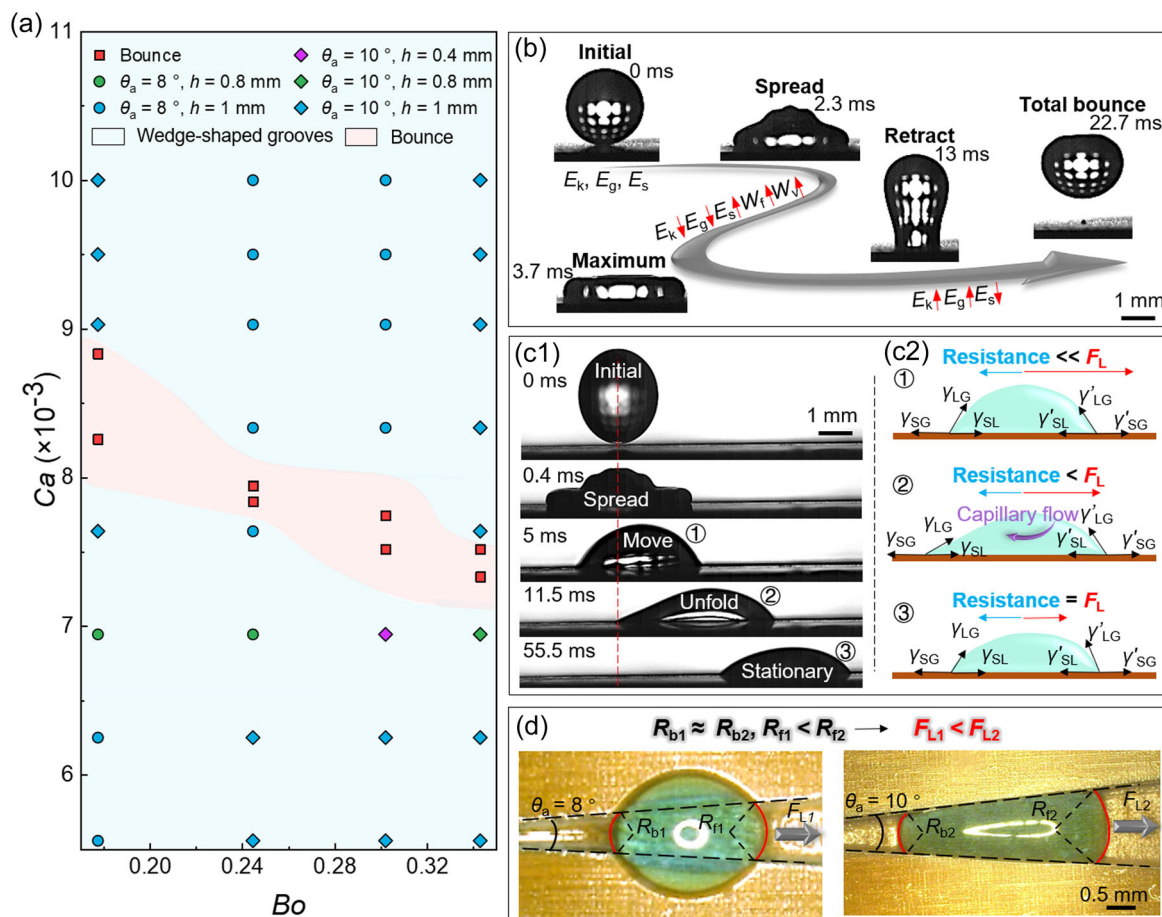


FIGURE 5 Optimal strategy and bouncing as well as transport mechanisms. (a) Strategy of efficient droplet separation from slippery liquid-infused porous surfaces. (b) Changing progress of the energy when the droplet impacts and bounces. (c1, c2) Schematic diagrams of the spontaneous transport mechanism. (d) Influence of θ_a on F_L .

Note that the left and right solid-liquid surface tension (γ_{SL} and γ'_{SL}) and solid-gas surface tension (γ_{SG} and γ'_{SG}) are equal at all times during the movement of the droplet. Therefore, the larger the depth, the faster the droplet will sink, thus promoting its movement. Figure 5d shows the influence of θ_a on F_L when $Ca = 0$ and $Bo = 0.18$. It can be seen that the radius of the back part (R_{b1} and R_{b2}) is similar, but the radius of the front part (R_{f1} and R_{f2}) increases as θ_a increases from 8° to 10° , so it can be stated that increasing θ_a helps to boost the driving force ($F_{L1} < F_{L2}$), thus promoting droplet movement.³⁷

Based on the best parameter combination discussed above, $\theta_a = 10^\circ$ and $h = 1$ mm were chosen to show the surface cleaning superiority of SLIPS with wedge-shaped grooves. As branched structures can aggregate droplets rapidly,^{23,38} functional SLIPS with primary and secondary branching wedge-shaped grooves for surface cleaning and droplet collection were created, where droplets of 1 mL were placed on secondary branches. It can be seen from Figure 6a that droplets successfully converge from the branches to the main road when droplets impact under a condition that is suitable for using $\theta_a = 10^\circ$ and $h = 1$ mm in Figure 5a. As droplets impact the SLIPS, droplets would always be deposited on the SLIPS, and after fusing, the bigger droplets just remain stable if there

are no wedge-shaped grooves, as shown in Figure 6b1 (Supporting Information: Movie S4). However, it can be seen from Figure 6b2 that droplets show a powerful transport ability on impacting SLIPS with wedge-shaped grooves, and as droplets continue to accumulate toward the central hole, large droplets will fuse and flow into the container (Supporting Information: Movie S5). After that, the residual volume is very small and there are residues in the groove, accumulating again with subsequent droplets. The process of continuous droplet impact and collection is succinctly illustrated in Figure 6c and the self-transport behavior of the droplets can be clearly observed in the Supporting Information: Movie S6. Although θ_a and h have been discussed sufficiently, parameters that also influence transport like impact position and liquid viscosity still need to be investigated in the future.

CONCLUSION

In summary, controllable self-transport of bouncing droplets on ultraslippery surfaces with wedge-shaped grooves was achieved in this work. It was found that hover, partial bounce, total bounce,

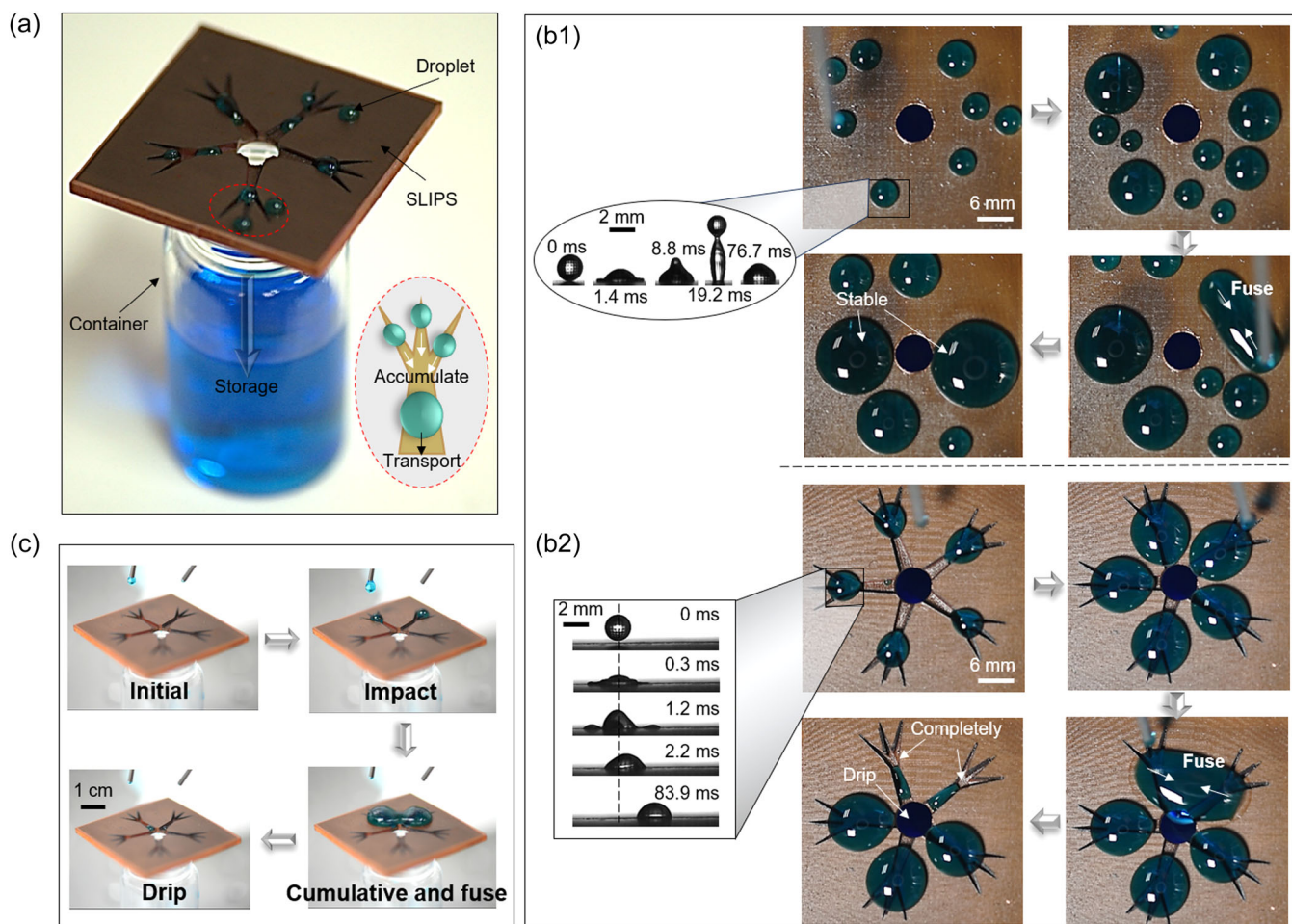


FIGURE 6 Design and application of slippery liquid-infused porous surfaces (SLIPS) for droplet transport. (a) Schematic diagram of SLIPS with branched grooves. (b1, b2) Comparison of the progress of droplet transport on SLIPS with wedge-shaped grooves and that on SLIPS with and without wedge-shaped grooves. (c) Progress of droplet impact and collection.

Worthington jet, and crush exist in sequence when droplets impact the SLIPS as the impact velocity increases. The influence of the wedge angle and groove depth on the design of wedge-shaped grooves was explored. The evolution of energy when droplets impact was clarified and a transport model was established to explain the mechanism. The branched structure with wedge-shaped grooves was chosen as an example of droplet self-transport, which shows an excellent effect. This work provides sufficient experimental and theoretical insights for spontaneous droplet motion control and improving the efficiency of surface cleaning.

METHODS

The substrate of all surfaces was copper, and the lubricant was silicone oil with viscosity $\mu_{\text{oil}} = 0.01 \text{ Pa s}$, surface tension $\gamma_{\text{oil}} = 0.021 \text{ N/m}$, and density $\rho_{\text{oil}} = 963 \text{ kg/m}^3$. The solution used for the chemical modification was a homogeneous mixture of 99 wt% anhydrous ethanol with a purity of 95% and 1 wt% 1H,1H,2H,2H-Perfluorodecyltrimethoxysilane ($\text{C}_{13}\text{H}_{13}\text{F}_{17}\text{O}_3\text{Si}$). Deionized water with viscosity $\mu_{\text{water}} = 0.001 \text{ Pa s}$,

surface tension $\gamma_{\text{water}} = 0.072 \text{ N/m}$, and density $\rho_{\text{water}} = 1000 \text{ kg/m}^3$ was used as the working fluid. Copper sheets were purchased from Suzhou Metal Material Manufacturer and all fluids were purchased from Aladdin.

The entire surface of a smooth copper sheet with dimensions of $40 \times 40 \times 2 \text{ mm}$ was scanned once using a UV-laser marking machine (KY-M-UV3L; Wuhan Keyi) at a speed of 1000 mm/s , power of 2 W , and a pulse frequency of 40 kHz to form micro-nano structures. After that, the sheet was immersed in a mixture solution of anhydrous ethanol and 1H,1H,2H,2H-Perfluorodecyltrimethoxysilane for 120 min to decreased the surface energy, and the superhydrophobic surface could be obtained after drying for 40 min at 100°C . With $30 \mu\text{L}$ of silicone oil dripped uniformly, SLIPS was obtained after tilting at 90° for 2 h to drain away excess silicone oil to avoid affecting the behavior of droplets. Based on the weighing method, the weight of residual oil was about 0.036 g and the experimental area on the copper sheet was $40 \times 40 \text{ mm}^2$, so the calculated residual oil film thickness was about 0.024 mm , which had a significant difference in magnitude compared to the diameter of water droplets (the scale is 1 mm). Therefore, the thickness of the oil film can be ignored, but it can still affect the impact behavior of droplets.

To fabricate wedge-shaped grooves on SLIPS, groove length $L = 30$ mm, groove depth $h = 0.2, 0.4, 0.6, 0.8$, and 1 mm, and wedge angle $\theta_a = 2, 4, 6, 8$, and 10° were chosen as parameters first. A layer of micro-nano structures was first machined on the surface of the copper specimen by UV-laser, and then wedge-shaped grooves were designed in the appropriate area. This ensured that all surfaces with droplet contact after the chemical modification and wetting operation were SLIPS.

The test environment was 25°C and the standard atmospheric pressure. The initial diameter $D_0 = 2.3, 2.7, 3$, and 3.2 mm and impact velocity U of droplets were controlled by the diameter of the syringe needle and its initial height (converting from Newton's first law and the required impact velocity), respectively. The syringe was plunged slowly so that droplets fell freely without initial velocity. The impact position was 5 mm far from the vertex of the groove. The whole impact process was recorded using a high-speed camera (i-SPEED 726R; iX Cameras) and analyzed using image processing software.

ACKNOWLEDGMENTS

The authors are grateful for the support from the National Natural Science Foundation of China (No. 51805252); Qingwen Dai acknowledges the support from the Alexander von Humboldt Foundation. Especially, Chuchen Yue thanks Kai Zhuang for critical discussions.

CONFLICT OF INTEREST STATEMENT

The authors declare no conflict of interest.

ORCID

Chuchen Yue  <http://orcid.org/0009-0002-6531-2470>

Qingwen Dai  <http://orcid.org/0000-0001-7422-4259>

Xiaolong Yang  <http://orcid.org/0000-0002-2324-6172>

Carsten Gachot  <http://orcid.org/0000-0001-6981-1563>

Wei Huang  <http://orcid.org/0000-0002-8871-634X>

Xiaolei Wang  <http://orcid.org/0000-0002-9055-1011>

REFERENCES

- Xu X, Li P, Ding Y, et al. Droplet energy harvesting panel. *Energy Environ Sci*. 2022;15:2916-2926.
- Yue C, Dai Q, Huang W, Wang X. Droplets bouncing on rotating curved surfaces with elevated temperatures. *Int J Heat Mass Transfer*. 2023;215:124479.
- Li H, Jin Q, Li H, et al. Transparent superamphiphobic material formed by hierarchical nano re-entrant structure. *Adv Funct Mater*. 2024;34:2309684.
- Xie Z, Jiao J, Wrona S. The fluid-structure interaction lubrication performances of a novel bearing: experimental and numerical study. *Tribol Int*. 2023;179:108151.
- Chen Y, Liu J, Song J, et al. Energy conversion based on superhydrophobic surfaces. *Phys Chem Chem Phys*. 2020;22:25430-25444.
- Hu S, Cao X, Reddyhoff T, et al. Pneumatic programmable super-repellent surfaces. *Droplet*. 2022;1:48-55.
- Dai Q, Yue C, Huang W, Wang X. Droplets impact on rotating cylinders. *Chem Eng Sci*. 2023;273:118669.
- Wu C, Qin X, Zheng H, et al. Self-adaptive droplet bouncing on a dual gradient surface. *Small*. 2023:2304635.
- Tang X, Saha A, Sun C, Law CK. Spreading and oscillation dynamics of drop impacting liquid film. *J Fluid Mech*. 2019;881:859-871.
- Zhang N, Gu H, Lu K, et al. A universal single electrode droplet-based electricity generator (SE-DEG) for water kinetic energy harvesting. *Nano Energy*. 2021;82:105735.
- Mouterde T, Lecointre P, Lehoucq G, Checco A, Clanet C, Quéré D. Two recipes for repelling hot water. *Nat Commun*. 2019;10:1410.
- Shi J, Zhang Y, Fan Y, Liu Y, Yang M. Recent advances in droplet-based microfluidics in liquid biopsy for cancer diagnosis. *Droplet*. 2024;3:e92.
- Sun P, Hao X, Jin Y, et al. Heterogenous slippery surfaces: enabling spontaneous and rapid transport of viscous liquids with viscosities exceeding 10 000 mPa s. *Small*. 2023;19:2304218.
- Wong T-S, Kang SH, Tang SKY, et al. Bioinspired self-repairing slippery surfaces with pressure-stable omniphobicity. *Nature*. 2011;477:443-447.
- Yang X, Zhuang K, Lu Y, Wang X. Creation of topological ultraslippery surfaces for droplet motion control. *ACS Nano*. 2021;15:2589-2599.
- Qi B, Yang X, Wang X. Ultraslippery/hydrophilic patterned surfaces for efficient fog harvest. *Colloids Surf A*. 2022;640:128398.
- Leng X, Sun L, Long Y, Lu Y. Bioinspired superwetting materials for water manipulation. *Droplet*. 2022;1:139-169.
- Wang N, Xiong D, Lu Y, et al. Design and fabrication of the lyophobic slippery surface and its application in anti-icing. *J Phys Chem C*. 2016;120:11054-11059.
- Wei C, Zhang G, Zhang Q, Zhan X, Chen F. Silicone oil-infused slippery surfaces based on sol-gel process-induced nanocomposite coatings: a facile approach to highly stable bioinspired surface for biofouling resistance. *ACS Appl Mater Interf*. 2016;8:34810-34819.
- Anand S, Paxson AT, Dhiman R, Smith JD, Varanasi KK. Enhanced condensation on lubricant-impregnated nanotextured surfaces. *ACS Nano*. 2012;6:10122-10129.
- Hui Guan J, Ruiz-Gutiérrez É, Xu BB, et al. Drop transport and positioning on lubricant-impregnated surfaces. *Soft Matter*. 2017;13:3404-3410.
- Launay G, Sadullah MS, McHale G, Ledesma-Aguilar R, Kusumaatmaja H, Wells GG. Self-propelled droplet transport on shaped-liquid surfaces. *Sci Rep*. 2020;10:14987.
- Zhang C, Zhang B, Ma H, et al. Bioinspired pressure-tolerant asymmetric slippery surface for continuous self-transport of gas bubbles in aqueous environment. *ACS Nano*. 2018;12:2048-2055.
- Chen S, Dai Q, Yang X, Liu J, Huang W, Wang X. Bioinspired functional structures for lubricant control at surfaces and interfaces: wedged-groove with oriented capillary patterns. *ACS Appl Mater Interf*. 2022;14:42635-42644.
- Zhuang K, Lu Y, Wang X, Yang X. Architecture-driven fast droplet transport without mass loss. *Langmuir*. 2021;37:12519-12528.
- Ruiz-Gutiérrez É, Guan JH, Xu B, McHale G, Wells GG, Ledesma-Aguilar R. Energy invariance in capillary systems. *Phys Rev Lett*. 2017;118:218003.
- Wang Z, Owais A, Neto C, Pereira J-M, Gan Y. Enhancing spontaneous droplet motion on structured surfaces with tailored wedge design. *Adv Mater Interf*. 2021;8:2000520.
- Li Y, Lu C, Liu Y. Directional transport of droplets impacting on superhydrophobic opening triangular groove surfaces. *J Phys Conf Ser*. 2022;2300:012002.
- Hao C, Li J, Liu Y, et al. Superhydrophobic-like tunable droplet bouncing on slippery liquid interfaces. *Nat Commun*. 2015;6:7986.
- Lee C, Kim H, Nam Y. Drop impact dynamics on oil-infused nanostructured surfaces. *Langmuir*. 2014;30:8400-8407.
- Chu F, Yan X, Miljkovic N. How superhydrophobic grooves drive single-droplet jumping. *Langmuir*. 2022;38:4452-4460.
- Yan X, Qin Y, Chen F, et al. Laplace pressure driven single-droplet jumping on structured surfaces. *ACS Nano*. 2020;14:12796-12809.
- Che Z, Deygas A, Matar OK. Impact of droplets on inclined flowing liquid films. *Phys Rev E*. 2015;92:023032.

34. Tao R, Liang G, Dou B, Wu J, Li B, Hao C. Oblique pancake bouncing. *Cell Rep Phys Sci*. 2022;3:100721.
35. Furmidge CGL. Studies at phase interfaces. I. The sliding of liquid drops on solid surfaces and a theory for spray retention. *J Colloid Sci*. 1962;17:309-324.
36. Balu B, Berry AD, Hess DW, Breedveld V. Patterning of super-hydrophobic paper to control the mobility of micro-liter drops for two-dimensional lab-on-paper applications. *Lab Chip*. 2009;9:3066-3075.
37. Liu W, Lu Y, Shen Y, Chen H, Ni Y, Xu Y. Spontaneous transport mechanics of water droplets under a synergistic action of designed pattern and non-wetting gradient. *ACS Omega*. 2023;8:16450-16458.
38. Liu Y, Xia Y, Zhan H, Lu C, Yuan Z, Zhao L. An electrothermal platform for active droplet manipulation. *RSC Adv*. 2023;13:14041-14047.

SUPPORTING INFORMATION

Additional supporting information can be found online in the Supporting Information section at the end of this article.

How to cite this article: Yue C, Dai Q, Yang X, Gachot C, Huang W, Wang X. Controllable self-transport of bouncing droplets on ultraslippery surfaces with wedge-shaped grooves. *Droplet*. 2024;3:e118. doi:10.1002/dro2.118